

ARTICLES

Long-range correlations in permeability fluctuations in porous rockHernán A. Makse,¹ Glenn W. Davies,² Shlomo Havlin,^{1,3} Plamen Ch. Ivanov,¹ Peter R. King,² and H. Eugene Stanley¹¹*Center for Polymer Studies and Department of Physics, Boston University, Boston, Massachusetts 02215*²*BP Exploration Operating Company Ltd., Sunbury-on-Thames, Middlesex, TW16 7LN, United Kingdom*³*Department of Physics, Bar-Ilan University, Ramat Gan, Israel*

(Received 5 December 1995; revised manuscript received 24 June 1996)

Porous media, such as sedimentary rocks, have complex permeability fluctuations arising from the physical processes that formed them. These permeability fluctuations significantly affect the flow of fluids through the rocks. We analyze data on two sandstone samples from different environments, and find that the permeability fluctuations display long-range power-law correlations characterized by an exponent $H > 1/2$. For both samples, we find similar values of H , $H \approx 0.82 - 0.90$, suggesting that the permeability in porous sandstone is not spatially uncorrelated as is generally assumed. [S1063-651X(96)11310-6]

PACS number(s): 64.60.Ak

I. INTRODUCTION

Granular materials are the objects of increasing interest for the physics community [1,2]. In particular, statistical physics has been a source of ideas, models, and techniques for studying static and dynamic properties of disordered and heterogeneous structures. Problems such as oil recovery and flow originating from the geophysical sciences [3] appear to be related to fluid flow in disordered media [4,5], percolation [6,7], fractals and lattice models [8], processes of diffusion [9], interfaces [10], scaling, self-affinity, and self-similarity of properties of porous media [11].

Permeability variations in disordered media such as sedimentary rocks are extremely important in predicting fluid flow in porous media. Permeability can change by many orders of magnitude over very short distances. Not only are there large fluctuations in permeability, but the permeability can exhibit strong spatial anisotropy. Deriving a mathematical representation to describe these spatial fluctuations in permeable rocks is a major challenge, and is also technologically important as efficient oil recovery depends on the ability to describe and predict flow through porous rock.

Hewett [12] has shown the existence of long-range spatial correlations in porosity values. Porosity is a measure of the *volume fraction of the void space*, while permeability is a *transport coefficient* relating flux to pressure gradient. For well-sorted, clean sands, porosity is independent of grain size while the permeability is proportional to the square of the particle radius. However, for poorly sorted nonclean sands, permeability is not a function of porosity alone [4,13]. Hence, it is not possible to predict permeability based on simple empirical correlations with porosity, since permeability may vary by several orders of magnitude for a given porosity [13]. Here, we study permeability values rather than porosity, because permeability directly affects fluid flow, and therefore it is more relevant than porosity when studying fluid flow in porous media.

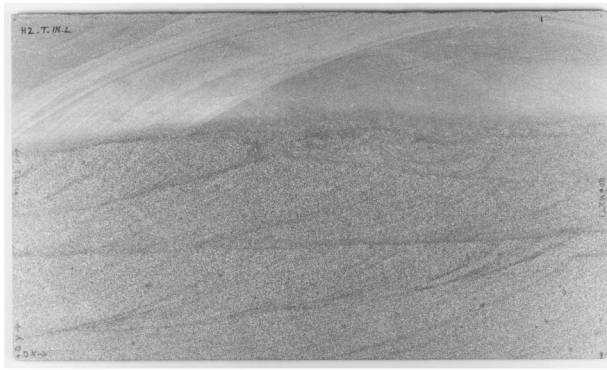
Only recently, the effects of correlations on the structure and dynamical properties of the media have been considered

in models of fluid flow in porous media [14] such as invasion percolation [15], and diffusion limited aggregation [16] in lattices whose occupied sites are correlated [17], and in percolation models [18,19]. Permeability fluctuations are traditionally modeled assuming correlations of finite range [20]. Long-range spatial correlations in permeability would affect the large-scale flow in a porous medium, so it is of practical as well as theoretical importance to distinguish between long-range and short-range correlations [21]. Here we analyze detailed permeability maps, and present experimental evidence for the existence of long-range correlations, which is relevant to some of these theoretical models.

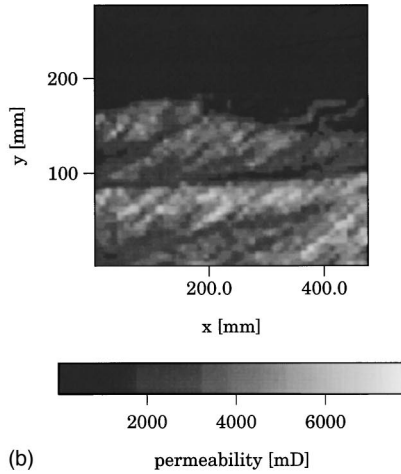
Specifically, we investigate two different sedimentary rock samples. One (denoted Ho) is *fluvial* sandstone from Hollington near Stafford in the East Midlands of England [13]. The second sample (denoted Lo) is *aeolian* sandstone from Locharbriggs near Dumfries, Scotland. Although the geological process is different for both samples, in both cases size segregation of particles occurs by avalanches—modified by fluid flow in the Ho case. We find the exponents characterizing the long-range correlations in the permeability values are the same, within errors bars, for both types of sandstone (fluvial and aeolian).

II. THE SAMPLES

Sample Ho, shown in Fig. 1, results from the migration of “sand bars” (accumulations of sand) along a river bed [3]. The current progressively moves sand from the upstream side of the sand accumulation to the downstream. On reaching the downstream side, the sand will roll down this face once a critical angle is exceeded. There is a degree of turbulence or eddying at the downstream face. This results from a higher flow rate at the top of the face and a lower rate at the base. Hence, grains toward the top of the downstream slope are better sorted, and so have lower packing. Those at the base are more poorly sorted, resulting from a mixture of larger grains rolling down the face and finer material dropping out of suspension. The degree of permeability contrast



(a)



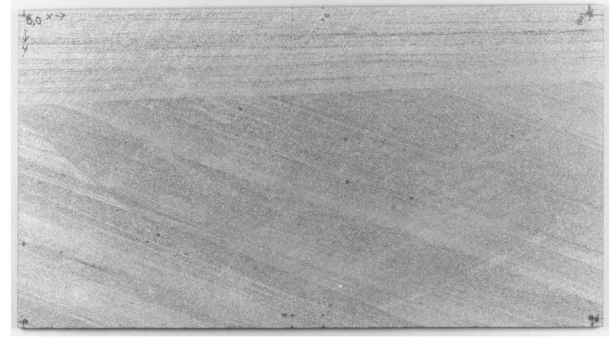
(b)

FIG. 1. (a) Photograph of one of the slabs for the sample Ho. The complete sample consists of two slabs, measuring 474 mm by 276 mm and 10 mm thick. Three faces at heights $z=0$, $z=10$, and $z=20$ mm were used to study the permeability pattern (the $z=0$ face is shown in this figure). Unfortunately the measurements of one face were corrupted by instrumentation error and so only three faces could be used. (b) Permeability map of (a). The permeability was measured every 10 mm in the x direction and every 4 mm in the y direction, so a grid of $n_x=48$ by $n_y=69$ permeability values was obtained.

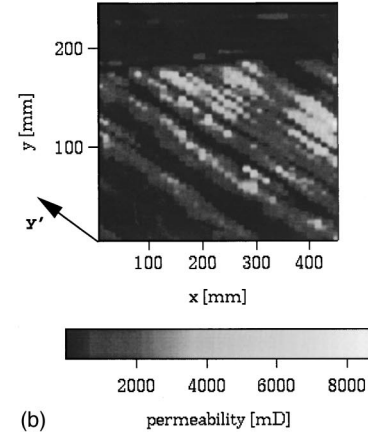
between the top and base of the bed depends on a combination of stream velocity, turbulence, and available grain sizes.

In Fig. 1 can be seen a sharp boundary between three regions. These represent where one sand bar has been overridden by another, partially eroding the top of the lower unit. This has occurred twice, as we can notice from the figure. Two of the zones are similar in character and have higher permeability, whereas the third has consistently lower permeability. We therefore treat the sample as having two zones of ‘high’ and one zone of ‘low’ permeability.

Sample Lo is shown in Fig. 2. The sedimentary rock was formed by windblown sand [22]. The wind transports the sand to the crest of the dune, and when the sand exceeds a critical angle it avalanches. In these avalanches the fine and coarse grains systematically segregate [23]. The resulting layers are clearly seen in Fig. 2. In this case the eddy fluid (air) on the downstream face has insufficient energy to influence the avalanching process, resulting in the face being planar rather than convex as in the fluvial sample. In this system, grain size range and permeability are relatively constant parallel to the laminations. Again, merging of dunes gives



(a)



(b)

FIG. 2. (a) Photograph of the face $z=0$ of the sample Lo. The complete sample consists of two slabs of 448 mm by 246 mm and 10 mm thick, and again only three faces were used in this study. (b) Permeability map of (a). The permeability was measured every 12 mm and 4 mm in the x and y directions, respectively, so that a grid of $n_x=38$ by $n_y=61$ was obtained. Notice the strong anisotropy of this sample manifested by the crests elongated along the y' direction.

rise to sharp transitions in permeability, so there are two zones. We notice also a strong spatial anisotropy in the high permeability zone of this sample.

III. CORRELATIONS

The minipermeameter is a tube through which a gas (air in laboratory measurements such as ours) is blown into the rock sample at a fixed pressure [24]. We use this technique to measure the permeability on the small scale of both rock samples. The flow rate of the gas into the rock sample is measured. The permeability k is then the ratio of the flow rate Φ to the pressure drop ΔP (which is applied pressure minus atmospheric pressure) multiplied by the viscosity of the gas μ ,

$$k \equiv -\frac{\mu\Phi}{\Delta P}. \quad (1)$$

Corrections must be made for the compressibility of the gas and the flow geometry, which is hemispherical from the injection point. The end of the permeameter in contact with the rock is made of a flexible plastic ring to ensure a good seal. The probe comes in a variety of sizes to measure per-

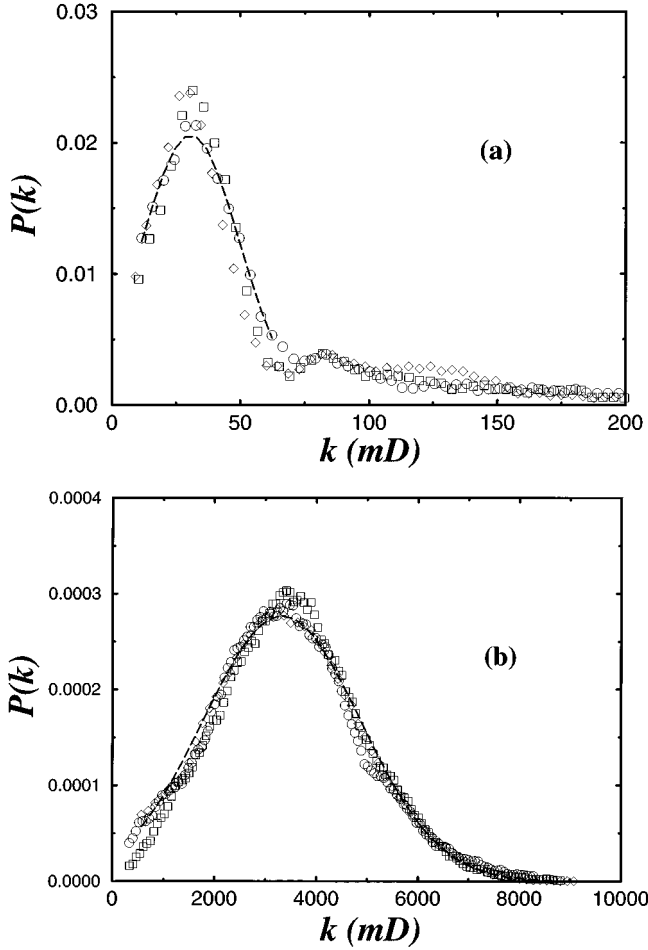


FIG. 3. Normalized permeability distributions for the sample Ho corresponding to (a) low permeability zone, and (b) high permeability zone. In both figures we plot the distributions corresponding to three different faces of the sample. The distributions are fitted by Gaussian functions. We notice the large difference in the mean value of the permeability between the low and high permeability zones.

meability fluctuations on different length scales; for our measurements the probe had a 1 cm diameter.

The permeability maps so obtained are shown in Figs. 1(b) and 2(b). By inspection, we see that local permeability varies significantly within a very short length scale, suggesting that the permeability may not be an independent random process.

We plot the permeability histograms for the sample Ho in Fig. 3. The high permeability zone has a typical permeability of 3300 mD, while the low permeability zone has a typical permeability of 30 mD. Local permeability is proportional to the square of the grain radius for uncompacted, well-sorted, clean, quartzite sandstone. The high permeability zone consists of interbedded fine and coarse grain material and hence has a much higher variability. The low permeability zone is more homogeneous, consisting of more exclusively fine grained material.

Next we measure the spatial correlations in permeability. We study the correlations of the permeability field $k(i, j)$ ($i, j = 1, \dots, n_x, n_y$) along the x and y directions [see Fig. 1(b)]. To this end, we first integrate the permeability vari-

ables along both directions separately, by calculating the “net displacements” $x_j(\ell)$ and $y_i(\ell)$,

$$x_j(\ell) \equiv \sum_{i=1}^{\ell} [k(i, j) - \overline{k(j)}] \quad (j = 1, \dots, n_y), \quad (2a)$$

and

$$y_i(\ell) \equiv \sum_{j=1}^{\ell} [k(i, j) - \overline{k(i)}] \quad (i = 1, \dots, n_x), \quad (2b)$$

where $\overline{k(j)} = (1/n_x) \sum_{i=1}^{n_x} k(i, j)$ and $\overline{k(i)} = (1/n_y) \times \sum_{j=1}^{n_y} k(i, j)$. The spatial average over a window of size ℓ is denoted by the overbar, and the disorder average over different displacements (x_j and y_i) is denoted by the angular brackets.

Next we calculate the variance

$$V_x(\ell) \equiv \langle \overline{x(\ell)^2} - \overline{x(\ell)}^2 \rangle^{1/2} \quad (3a)$$

and

$$V_y(\ell) \equiv \langle \overline{y(\ell)^2} - \overline{y(\ell)}^2 \rangle^{1/2} \quad (3b)$$

as a function of the lag ℓ . The scaling behavior of the variance

$$V_x(\ell) \sim \ell^{H_x}, \quad V_y(\ell) \sim \ell^{H_y} \quad (4)$$

can distinguish between short- and long-range correlations since for uncorrelated permeability variables, $H = 1/2$, while $1/2 < H < 1$ implies persistent long-range correlations among the variables. The correlation exponent H describes the “roughness of the permeability landscape” [11], and is usually called the Hurst exponent for the associated fractional Brownian motion (fBm) [25] $x_j(\ell)$ and $y_i(\ell)$ defined by Eq. (2). However, we note that the original permeability $k(i, j)$ is fractional Gaussian noise (fGn) [25,26]. Therefore, in a numerical study of the effect of long-range correlations in porous media, one must generate the permeability values from a fGn [19] and not from a fBm [14]. A method to generate long-range correlated variables for large systems is described in [27].

The method described so far is called rms fluctuation analysis which, however, is known to fail if (i) the signal is nonstationary [28], or (ii) the signal is highly correlated $H \approx 1$ [29]. In case (i), the rms method detects spurious correlations due to the patchiness of the signal [28], while in case (ii) the rms method gives smaller effective exponents (in particular when small samples are used) because the variance has an upper bound $V(\ell) < \ell$ and therefore the method cannot detect fluctuations with exponent $H \geq 1$ [29]. In our case we find that, apart from possible nonstationarities, the permeability values are strongly correlated.

To overcome the limitations of the rms method, we will analyze the spatial correlations of the permeability by using detrended fluctuation analysis (DFA) [28] and wavelet analysis [30]. The DFA method [28] consists of subtracting the local trend (defined as the ordinate of a linear least-squares fit to the permeability values) in each window of size ℓ defined in (2).

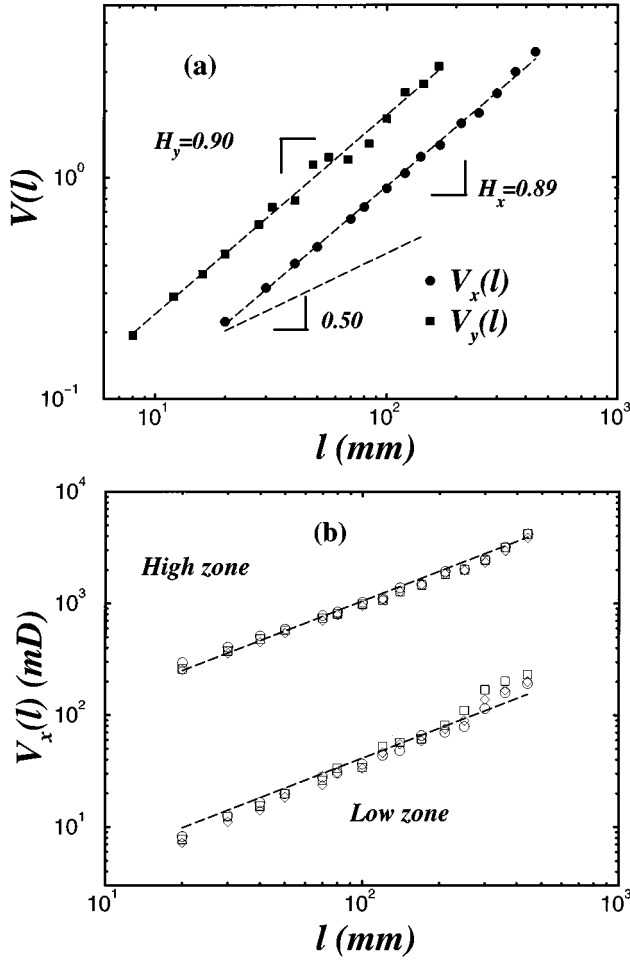


FIG. 4. Log-log plot of the normalized variances of the permeability calculated using the DFA method. (a) Variances $V_x(\ell)$ and $V_y(\ell)$ along the x and y directions, respectively, averaged over the three different faces of the sample, and averaged over the high and low permeability zones together for $V_x(\ell)$, and over the high permeability zone for $V_y(\ell)$. The power-law relationship between the variance and the separation distance ℓ is characterized by exponents $H_x = 0.89 \pm 0.06$ and $H_y = 0.90 \pm 0.06$. The exponents are the same within error bars indicating the isotropy of the correlations in the xy plane. (b) Variance $V_x(\ell)$ calculated along the x direction for the high and low permeability zones, separately. Data are averaged over the three different faces of the sample. Both sets of data are consistent with a power law $H_x \approx 0.89$, showing that the spatial correlations are the same in both zones.

The wavelet transform (WT) of a given function $f(x)$ is defined as

$$T_\Psi(x_0, a) \equiv \frac{1}{a} \int_{-\infty}^{\infty} f(x) \Psi\left(\frac{x-x_0}{a}\right) dx, \quad (5)$$

where Ψ is the analyzing wavelet, x_0 the translation parameter, and a the scale parameter. After performing the WT with a wavelet analyzer given by the first derivative of the Gaussian function, we can determine the values $x_i(a)$ at which T_Ψ has local extrema. The sum of the absolute values of the local extrema raised to the power q exhibits power-law dependence on the scale a ,

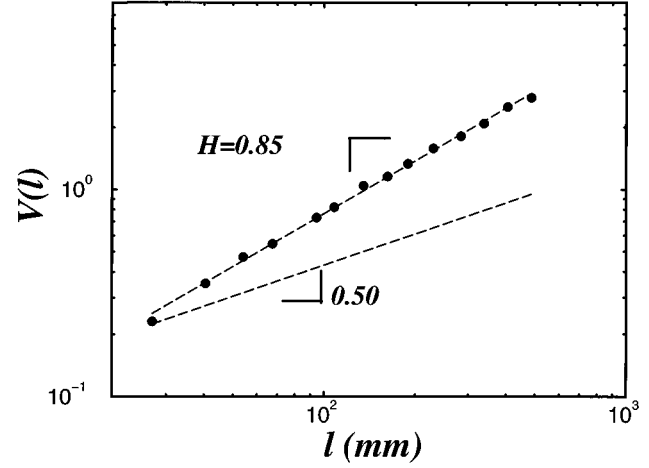


FIG. 5. Log-log plot of the normalized variance calculated along the y' for the high permeability zone of sample Lo, averaged over the three different faces of the sample. Along the y' direction, a correlation exponent of $H = 0.85 \pm 0.06$ is found. However, along the x' direction, a periodic pattern is observed. Thus the anisotropy in this sample is manifested in a change of behavior from long-range correlation scaling along y' to periodic morphology along x' .

$$Z(a, q) \equiv \sum_{\{x_i(a)\}} |T_\Psi(x_i(a), a)|^q \sim a^{\tau(q)}, \quad (6)$$

defining the exponent $\tau(q)$.

The function $Z(a, q)$ is directly related to the scaling properties of the q th moment of the signal $f(x)$. For certain values of q , the exponents $\tau(q)$ have known meaning. In particular $\tau(2)$ is related to the scaling exponent of the Fourier power spectra: $S(f) \sim f^{-\beta}$ with $\beta = 2 + \tau(2)$, and therefore

$$\tau(2) = 2H - 1. \quad (7)$$

Thus $\tau(2) > 0$ indicates the presence of long-range correlations ($H > 1/2$), and $\tau(2) = 0$ ($H = 1/2$) indicate the absence of correlations. The wavelet method is free from restrictions related to nonstationarities and to the presence of large correlations [30]. The elimination of nonstationarities from the signal — accomplished by the wavelet transform — is important since the observation of an exponent $H > 1/2$ might be an artifact of a systematic smooth variation, or linear trend ($H = 1$) in the data plus the effects of random fluctuations ($H = 1/2$). In this case a nonstationarity in the signal might be confused with the existence of long-range correlations.

The results for the permeability correlations for the sample Ho are shown in Fig. 4. In Fig. 4(a), we show the correlations for both high and low permeability zones, measured in the x and y directions. In this case, before calculating the variance, the permeability is normalized by dividing by the standard deviation calculated independently for each direction. The data are consistent with power-law correlations; using the DFA method, we find

$$H_x = 0.89 \pm 0.06, \quad H_y = 0.90 \pm 0.06 \quad (\text{Ho: DFA}). \quad (8a)$$

Results for the correlations along the x direction are shown separately for the high and low permeability zones in Fig. 4(b). The correlations are satisfactorily modeled by a power law with $H_x \approx 0.89$, independent of the magnitude of the overall permeability. These values are confirmed, within the error bars, using the wavelet analysis. We find that

$$H_x = 0.82 \pm 0.06, \quad H_y = 0.84 \pm 0.06 \quad (\text{Ho: Wavelet}). \quad (8b)$$

As seen in Fig. 2, the high permeability zone of sample Lo presents strong anisotropy with anisotropic axes (x', y') not coincident with the coordinate frame (x, y) [see Fig. 2(b)]. We calculate the variance along the y' direction (parallel to the direction of the crests) and find (Fig. 5) using the DFA method

$$H_{y'} = 0.85 \pm 0.06 \quad (\text{Lo: DFA}) \quad (9a)$$

a value that is consistent with our findings for the sample Ho. Using wavelet analysis, we find

$$H_{y'} = 0.84 \pm 0.06 \quad (\text{Lo: Wavelet}). \quad (9b)$$

Along the x' direction a periodic morphology is observed with a wavelength of about 60 mm. This introduces a characteristic length scale so that no scale invariance power-law correlations are expected along this direction. The existence of this laminar periodic structure is consistent with a depositional model of sand dune dynamics [23].

Thus for both methods we find that $H > 1/2$, thereby demonstrating the presence of long-range correlations in the Ho and Lo samples. The fact that we find no upper cutoff in the

variances plotted in Figs. 4 and 5 indicates that the correlations might extend beyond the length of the samples used in this study. However, it should be noted that at larger length scales the nature of the correlations might be modified by the stratified structure of the rock [31].

IV. DISCUSSION

Spatial fluctuations in rock permeability exist, and require quantitative methods to describe them. We have shown that permeability correlations in two different rock samples are scale invariant and can be well described using a power-law. Further, the exponent is quite similar for the two samples studied, Ho and Lo. The essential physical feature in the formation of these two samples is avalanching of the sand grains, which gives rise to segregation and alternation in the fine and coarse material [23]. It is possible that this mechanism may explain the apparent universality in the power-law correlations for these rock types. These spatial fluctuations have significant consequences for prediction of, e.g., oil recovery in reservoir rocks. For example, the fact that there exist long-range correlations implies that the spread in contaminant transport could be much faster ("enhanced diffusion" [32]) than would be predicted from a short-range correlation model.

ACKNOWLEDGMENTS

The authors thank BP Exploration Operating Company for financial support and permission to publish this paper, and S. Tomassone for valuable discussions. S.H. thanks the Israel Science Foundation for financial support.

-
- [1] D. Bideaux and A. Hansen, *Disorder and Granular Media* (North-Holland, Amsterdam, 1993).
 - [2] D. E. Wolf, in *Computational Physics: Selected Methods – Simple Exercises – Serious Applications*, edited by K. H. Hoffmann and M. Schreiber (Springer-Verlag, Heidelberg, 1996).
 - [3] J. R. L. Allen, *Principles of Physical Sedimentology* (George Allen and Unwin, London, 1985).
 - [4] M. Sahimi, *Rev. Mod. Phys.* **65**, 1393 (1993); M. Sahimi, *Applications of Percolation Theory* (Taylor & Francis, London, 1994); F. Family and M. Sahimi, *Fractals in Materials Science* (Oxford University Press, London, 1996).
 - [5] J. S. Andrade, Jr., D. A. Street, T. Shinohara, Y. Shibusa, and Y. Arai, *Phys. Rev. E* **51**, 5725 (1995).
 - [6] *Fractals and Disordered Systems*, 2nd ed., edited by A. Bunde and S. Havlin (Springer-Verlag, Heidelberg, 1996).
 - [7] D. Stauffer and A. Aharony, *Introduction to Percolation Theory* (Taylor & Francis, London, 1992).
 - [8] T. Vicsek, *Fractal Growth Phenomena*, 2nd ed. (World Scientific, Singapore, 1989).
 - [9] S. Havlin and D. Ben-Avraham, *Adv. Phys.* **36**, 695 (1987).
 - [10] P. Meakin, *Phys. Rep.* **235**, 189 (1993); A.-L. Barabási and H. E. Stanley, *Fractal Concepts in Surface Growth* (Cambridge University Press, Cambridge, 1995).
 - [11] *Dynamics of Fractal Surfaces*, edited by F. Family and T. Vicsek (World Scientific, Singapore, 1991).
 - [12] T. A. Hewett (unpublished); T. A. Hewett and R. A. Behrens, *SPE Formation Evaluation* **5**, 217 (1990).
 - [13] A. C. Brayshaw, G. W. Davies, and P. W. M. Corbett, in *Advances in Fluvial Dynamics and Stratigraphy*, edited by P.A. Carling and M.R. Dawson (Wiley, New York, 1996).
 - [14] M. Sahimi, *J. Phys. (France) I* **4**, 1263 (1994); M. Sahimi and M. A. Knackstedt, *ibid.* **4**, 1269 (1994); M. Sahimi, *AIChE J.* **41**, 229 (1995).
 - [15] C. Du, B. Xu, Y. C. Yortsos, M. Chaouche, N. Rakotomalala, and D. Salin, *Phys. Rev. Lett.* **74**, 694 (1995).
 - [16] T. A. Witten and L. M. Sander, *Phys. Rev. Lett.* **47**, 1400 (1981).
 - [17] K. B. Lauritsen, M. Sahimi, and H. J. Herrmann, *Phys. Rev. E* **48**, 1272 (1993).
 - [18] A. Weinrib, *Phys. Rev. B* **29**, 387 (1984).
 - [19] S. Prakash, S. Havlin, M. Schwartz, and H. E. Stanley, *Phys. Rev. A* **46**, R1724 (1992).
 - [20] L. Smith and F. W. Schwartz, *Water Resour. Res.* **16**, 303 (1979).
 - [21] S. Havlin, R. Selinger, M. Schwartz, H. E. Stanley, and A. Bunde, *Phys. Rev. Lett.* **61**, 1438 (1988).
 - [22] R. A. Bagnold, *The Physics of Blown Sand and Desert Dunes* (Chapman and Hall, London, 1941).
 - [23] H. A. Makse, S. Havlin, P. R. King, and H. E. Stanley (unpublished); P.-G. de Gennes, *J. Phys. (France) I* (to be published).
 - [24] C. Halvorsen and A. Hurst, in *Advances in Core Evaluation*

- Accuracy and Prediction*, edited by P. F. Worthington (Gordon and Breach, London, 1990).
- [25] B. B. Mandelbrot and J. W. Van Ness, *SIAM Rev.* **10**, 442 (1968).
- [26] Fractional Gaussian noise corresponds to the increments of the fBm [25]. For instance, according to Eq. (2a), $k(\ell) - \bar{k} = x(\ell) - x(\ell-1)$ is a fGn, and $x(\ell)$ is a fBm (for a fixed value of j).
- [27] H. Makse, S. Havlin, M. Schwartz, and H. E. Stanley, *Phys. Rev. E* **53**, 5445 (1996).
- [28] C. K. Peng, S. V. Buldyrev, S. Havlin, M. Simons, H. E. Stanley, and A. L. Goldberger, *Phys. Rev. E* **49**, 1685 (1994).
- [29] H. Leschhorn and L.-H. Tang, *Phys. Rev. Lett.* **70**, 2973 (1993); H. A. Makse and L. A. N. Amaral, *Europhys. Lett.* **31**, 379 (1995).
- [30] J. F. Muzy, E. Bacry, and A. Arneodo, *Phys. Rev. Lett.* **67**, 3515 (1991); A. Arneodo, E. Bacry, P. V. Graves, and J. F. Muzy, *ibid.* **74**, 3292 (1995); P. Ch. Ivanov, M. G. Rosenblum, C.-K. Peng, J. Mietus, S. Havlin, H. E. Stanley, and A. L. Goldberger, *Nature* (to be published).
- [31] M. Sahimi, H. Rassamdana, and A. Mehrabi, in *Fractal Aspects of Materials: Materials Research Society Symposia Proceedings* No. 367 (MRS, Pittsburgh, 1995), p. 203.
- [32] M. F. Shlesinger and J. Klafter, *Phys. Rev. Lett.* **54**, 2551 (1985).